Single-step fabrication process of 1-D photonic crystals coupled to nanocolumnar TiO_2 layers to improve DSC efficiency

L. González-García,[1,2,3] S. Colodrero,[1,2,4] H. Míguez,[1] and A. R. González-Elipe[1,*]

[1]*Instituto de Ciencia de Materiales, CSIC-Universidad de Sevilla, Américo Vespucio 49, 41092 Sevilla, Spain*
[2]*These authors contributed equally to this work*
[3]*Present address: INM–Leibniz Institute for New Materials, Campus D2 2, 66123 Saarbrücken, Germany*
[4]*Present address: ICFO–Institut de Ciencies Fotoniques, Mediterranean Technology Park, 08860 Castelldefels, Spain*
[*]*arge@icmse.csic.es*

Abstract: The present work proposes the use of a TiO_2 electrode coupled to a one-dimensional photonic crystal (1DPC), all formed by the sequential deposition of nanocolumnar thin films by physical vapor oblique angle deposition (PV-OAD), to enhance the optical and electrical performance of DSCs while transparency is preserved. We demonstrate that this approach allows building an architecture combining a non-dispersive 3 μm of TiO_2 electrode and 1 μm TiO_2-SiO_2 1DPC, both columnar, in a single-step process. The incorporation of the photonic structure is responsible for a rise of 30% in photovoltaic efficiency, as compared with a transparent cell with a single TiO_2 electrode. Detailed analysis of the spectral dependence of the photocurrent demonstrates that the 1DPC improves light harvesting efficiency by both back reflection and optical cavity modes confinement within the TiO_2 films, thus increasing the overall performance of the cell.

OCIS codes: (160.0160) Materials; (160.5298) Photonic crystals; (230.0230) Optical devices; (230.4170) Multilayers; (310.0310) Thin films; (310.1860) Deposition and fabrication.

References and links

1. B. O'Regan and M. Gratzel, "A low-cost, high-efficiency solar-cell based on dye-sensitized colloidal TiO2 Films," Nature **353**(6346), 737–740 (1991).
2. D. Colonna, S. Colodrero, H. Lindstrom, A. Di Carlo, and H. Miguez, "Introducing structural colour in DSCs by using photonic crystals: interplay between conversion efficiency and optical properties," Energy Environ. Sci. **5**(8), 8238–8243 (2012).
3. M. Law, L. E. Greene, J. C. Johnson, R. Saykally, and P. Yang, "Nanowire dye-sensitized solar cells," Nat. Mater. **4**(6), 455–459 (2005).
4. E. Galoppini, J. Rochford, H. Chen, G. Saraf, Y. Lu, A. Hagfeldt, and G. Boschloo, "Fast electron transport in metal organic vapor deposition grown dye-sensitized ZnO nanorod solar cells," J. Phys. Chem. B **110**(33), 16159–16161 (2006).
5. A. B. F. Martinson, J. E. McGarrah, M. O. K. Parpia, and J. T. Hupp, "Dynamics of charge transport and recombination in ZnO nanorod array dye-sensitized solar cells," Phys. Chem. Chem. Phys. **8**(40), 4655–4659 (2006).
6. I. Gonzalez-Valls and M. Lira-Cantu, "Vertically-aligned nanostructures of ZnO for excitonic solar cells: a review," Energy Environ. Sci. **2**(1), 19–34 (2009).
7. B. Liu and E. S. Aydil, "Growth of oriented single-crystalline rutile TiO2 nanorods on transparent conducting substrates for dye-sensitized solar cells," J. Am. Chem. Soc. **131**(11), 3985–3990 (2009).
8. L. Gonzalez-Garcia, I. Gonzalez-Valls, M. Lira-Cantu, A. Barranco, and A. R. Gonzalez-Elipe, "Aligned TiO2 nanocolumnar layers prepared by PVD-GLAD for transparent dye sensitized solar cells," Energy Environ. Sci. **4**(9), 3426–3435 (2011).
9. L. M. Peter, "Characterization and modeling of dye-sensitized solar cells," J. Phys. Chem. C **111**(18), 6601–6612 (2007).
10. G. K. Kiema, M. J. Colgan, and M. J. Brett, "Dye sensitized solar cells incorporating obliquely deposited titanium oxide layers," Sol. Energy Mater. Sol. Cells **85**(3), 321–331 (2005).
11. H.-Y. Yang, M.-F. Lee, C.-H. Huang, Y.-S. Lo, Y.-J. Chen, and M.-S. Wong, "Glancing angle deposited titania films for dye-sensitized solar cells," Thin Solid Films **518**(5), 1590–1594 (2009).

#245708 Received 9 Jul 2015; revised 9 Sep 2015; accepted 5 Oct 2015; published 3 Nov 2015

12. L. Gonzalez-Garcia, J. Idigoras, A. R. Gonzalez-Elipe, A. Barranco, and J. A. Anta, "Charge collection properties of dye-sensitized solar cells based on 1-dimensional TiO_2 porous nanostructures and ionic-liquid electrolytes," J. Photochem. Photobio. A-Chemistry **241**, 58–66 (2012).
13. Q. Zhang, T. P. Chou, B. Russo, S. A. Jenekhe, and G. Cao, "Aggregation of ZnO nanocrystallites for high conversion efficiency in dye-sensitized solar cells," Angew. Chem. Int. Ed. Engl. **47**(13), 2402–2406 (2008).
14. C. Y. Jiang, X. W. Sun, G. Q. Lo, D. L. Kwong, and J. X. Wang, "Improved dye-sensitized solar cells with a ZnO-nanoflower photoanode," Appl. Phys. Lett. **90**(26), 263501 (2007).
15. A. Usami, "Theoretical study of application of multiple scattering of light to a dye-sensitized nanocrystalline photoelectrochemical cell," Chem. Phys. Lett. **277**(1-3), 105–108 (1997).
16. A. Yella, H.-W. Lee, H. N. Tsao, C. Yi, A. K. Chandiran, M. K. Nazeeruddin, E. W.-G. Diau, C.-Y. Yeh, S. M. Zakeeruddin, and M. Grätzel, "Porphyrin-sensitized solar cells with cobalt (II/III)-Based redox electrolyte exceed 12 percent efficiency," Science **334**(6056), 629–634 (2011).
17. F. E. Gálvez, E. Kemppainen, H. Míguez, and J. Halme, "Effect of diffuse light scattering designs on the efficiency of dye solar cells: an integral optical and electrical description," J. Phys. Chem. C **116**(21), 11426–11433 (2012).
18. Q. Zhang, D. Myers, J. Lan, S. A. Jenekhe, and G. Cao, "Applications of light scattering in dye-sensitized solar cells," Phys. Chem. Chem. Phys. **14**(43), 14982–14998 (2012).
19. S. Nishimura, N. Abrams, B. A. Lewis, L. I. Halaoui, T. E. Mallouk, K. D. Benkstein, J. van de Lagemaat, and A. J. Frank, "Standing wave enhancement of red absorbance and photocurrent in dye-sensitized titanium dioxide photoelectrodes coupled to photonic crystals," J. Am. Chem. Soc. **125**(20), 6306–6310 (2003).
20. A. Mihi and H. Míguez, "Origin of light-harvesting enhancement in colloidal-photonic-crystal-based dye-sensitized solar cells," J. Phys. Chem. B **109**(33), 15968–15976 (2005).
21. A. Mihi, M. E. Calvo, J. A. Anta, and H. Miguez, "Spectral response of opal-based dye-sensitized solar cells," J. Phys. Chem. C **112**(1), 13–17 (2008).
22. S. Colodrero, A. Mihi, L. Haggman, M. Ocana, G. Boschloo, A. Hagfeldt, and H. Miguez, "Porous One-dimensional photonic crystals improve the power-conversion efficiency of dye-sensitized solar cells," Adv. Mater. **21**(7), 764–770 (2009).
23. S. Colodrero, A. Mihi, J. A. Anta, M. Ocana, and H. Miguez, "Experimental demonstration of the mechanism of light harvesting enhancement in photonic-crystal-based dye-sensitized solar cells," J. Phys. Chem. C **113**(4), 1150–1154 (2009).
24. M. Guo, K. Xie, J. Lin, Z. Yong, C. T. Yip, L. Zhou, Y. Wang, and H. Huang, "Design and coupling of multifunctional TiO_2 nanotube photonic crystal to nanocrystalline titania layer as semi-transparent photoanode for dye-sensitized solar cell," Energy Environ. Sci. **5**(12), 9881 (2012).
25. M. E. Calvo, S. Colodrero, N. Hidalgo, G. Lozano, C. López-López, O. Sánchez-Sobrado, and H. Míguez, "Porous one dimensional photonic crystals: novel multifunctional materials for environmental and energy applications," Energy Environ. Sci. **4**(12), 4800 (2011).
26. A. Mihi, C. Zhang, and P. V. Braun, "Transfer of preformed three-dimensional photonic crystals onto dye-sensitized solar cells," Angew. Chem. Int. Ed. Engl. **50**(25), 5712–5715 (2011).
27. S. K. Karuturi, C. Cheng, L. Liu, L. Tat Su, H. J. Fan, and A. I. Y. Tok, "Inverse opals coupled with nanowires as photoelectrochemical anode," Nano Energy **1**(2), 322–327 (2012).
28. M. Guo, Z. Yong, K. Xie, J. Lin, Y. Wang, and H. Huang, "Enhanced light harvesting in dye-sensitized solar cells coupled with titania nanotube photonic crystals: a theoretical study," ACS Appl. Mater. Interfaces **5**(24), 13022–13028 (2013).
29. C. T. Yip, H. Huang, L. Zhou, K. Xie, Y. Wang, T. Feng, J. Li, and W. Y. Tam, "Direct and seamless coupling of TiO2 nanotube photonic crystal to dye-sensitized solar cell: a single-step approach," Adv. Mater. **23**(47), 5624–5628 (2011).
30. L. González-García, J. Parra-Barranco, J. R. Sánchez-Valencia, A. Barranco, A. Borrás, A. R. González-Elipe, M. C. García-Gutiérrez, J. J. Hernández, D. R. Rueda, and T. A. Ezquerra, "Correlation lengths, porosity and water adsorption in TiO_2 thin films prepared by glancing angle deposition," Nanotechnology **23**(20), 205701 (2012).
31. L. Gonzalez-Garcia, G. Lozano, A. Barranco, H. Miguez, and A. R. Gonzalez-Elipe, "TiO_2-SiO_2 one-dimensional photonic crystals of controlled porosity by glancing angle physical vapour deposition," J. Mater. Chem. **20**(31), 6408–6412 (2010).
32. M. Oliva-Ramirez, L. González-García, J. Parra-Barranco, F. Yubero, A. Barranco, and A. R. González-Elipe, "Liquids analysis with optofluidic bragg microcavities," ACS Appl. Mater. Interfaces **5**(14), 6743–6750 (2013).
33. M. E. Calvo, L. González-García, J. Parra-Barranco, A. Barranco, A. Jiménez-Solano, A. R. González-Elipe, and H. Míguez, "Flexible distributed Bragg reflectors from nanocolumnar templates," Adv. Opt. Mater. **3**(2), 171–175 (2015).
34. A. Barranco, A. Borras, A. R. Gonzalez-Elipe, and A. Palmero, "Perspectives on oblique angle deposition for thin films: From fundamentasl to devices," Prog. Mater. Sci. (2015), doi:10.1016/j.pmatsci.2015.06.003.
35. K. Robbie, M. J. Brett, and A. Lakhtakia, "Chiral sculptured thin films," Nature **384**(6610), 616 (1996).
36. M. M. Hawkeye and M. J. Brett, "Glancing angle deposition: fabrication, properties, and applications of micro- and nanostructured thin films," J. Vac. Sci. Technol. A **25**(5), 1317–1335 (2007).
37. M. J. Brett and M. M. Hawkeye, "Materials science. New materials at a glance," Science **319**(5867), 1192–1193 (2008).
38. L. González-García, A. Barranco, A. M. Páez, A. R. González-Elipe, M. C. García-Gutiérrez, J. J. Hernández, D. R. Rueda, T. A. Ezquerra, and D. Babonneau, "Structure of glancing incidence deposited TiO(2) thin films as revealed by grazing incidence small-angle X-ray scattering," Chem. Phys. Chem. **11**(10), 2205–2208 (2010).

#245708 Received 9 Jul 2015; revised 9 Sep 2015; accepted 5 Oct 2015; published 3 Nov 2015

39. K. M. Krause, M. T. Taschuk, K. D. Harris, D. A. Rider, N. G. Wakefield, J. C. Sit, J. M. Buriak, M. Thommes, and M. J. Brett, "Surface area characterization of obliquely deposited metal oxide nanostructured thin films," Langmuir **26**(6), 4368–4376 (2010).
40. K. Kaminska, M. Suzuki, K. Kimura, Y. Taga, and K. Robbie, "Simulating structure and optical response of vacuum evaporated porous rugate filters," J. Appl. Phys. **95**(6), 3055–3062 (2004).
41. K. D. Harris, D. Vick, E. J. Gonzalez, T. Smy, K. Robbie, and M. J. Brett, "Porous thin films for thermal barrier coatings," Surf. Coat. Tech. **138**(2-3), 185–191 (2001).
42. S. Colodrero, A. Forneli, C. Lopez-Lopez, L. Pelleja, H. Miguez, and E. Palomares, "Efficient transparent thin dye solar cells based on highly porous 1D photonic crystals," Adv. Funct. Mater. **22**(6), 1303–1310 (2012).
43. C. Lopez-Lopez, S. Colodrero, S. R. Raga, H. Lindstrom, F. Fabregat-Santiago, J. Bisquert, and H. Miguez, "Enhanced diffusion through porous nanoparticle optical multilayers," J. Mater. Chem. **22**(5), 1751–1757 (2012).
44. G. Lozano, S. Colodrero, O. Caulier, M. E. Calvo, and H. Miguez, "Theoretical analysis of the performance of one-dimensional photonic crystal-based dye-sensitized solar cells," J. Phys. Chem. C **114**(8), 3681–3687 (2010).
45. L. Pavesi, "Porous silicon dielectric multilayers and microcavities," Riv. Nuovo Cim. **20**(10), 1–76 (1997).

1. Introduction

The depletion of fossil fuels and the rising energy demand have kindled worldwide the research interest in new technologies to exploit clean energy sources such as solar light, wind, water, hydrogen, etc. Within this context, production of electric energy using versatile photovoltaic cells is an appealing choice. Since the pioneering work of O'Regan and Grätzel in 1991 [1], dye sensitized solar cells (DSCs) have attracted a great interest due to their low cost, high energy conversion efficiency, simple fabrication process and transparency. In particular, this latter characteristic implies an outstanding application benchmark for building-integrated photovoltaics (BIPV) applications [2].

In the race for improving the efficiency of these devices, a widespread strategy consists of using electrodes formed by 1-dimensional (1-D) nanostructures, such as nanowires and nanotubes [3–8]. The main advantage of such architectures lies in an improved collection of charge resulting from a direct path of electrons up to the external circuit, the minimization of the charge recombination processes at the grain boundaries and a limited exposure to the electron acceptors of the electrolyte [9]. Examples of this type of DSC configuration can be found in previous studies using nanocolumnar structures prepared by physical vapor oblique angle deposition (PV-OAD), where maximum efficiencies of ca. 3% and 4% have been reported for TiO_2 anodes with thicknesses of 2.5 and 10 μm, respectively [8, 10–12]. In this case, the equivalent or slightly lower power conversion efficiencies obtained for these devices when compared to those based on nanoparticle electrodes [13] have been attributed to a lower surface area available for dye adsorption, which gives rise to low values of light harvesting efficiency (LHE) [13, 14]. Improved designs should therefore solve this issue by either increasing the effective surface area or modifying the optical design of the structure. In this regard, LHE in DSCs with standard electrodes made of nanocrystalline titania has been improved by the incorporation of diffuse back scattering layers [15–18]. Unfortunately, this configuration also leads to an undesirable loss of transparency of the final device. A compromise between transparency and enhancement of LHE has been reached by incorporating different porous photonic crystals (PCs) onto the TiO_2 electrode, being inverse opals [19–21] and multilayers [22–24] the most widely employed. These structures produce the reflection of light within a well-defined wavelength range, hence increasing the probability of light absorption by the photoactive layer, while allowing the rest of wavelengths to be transmitted [20, 25]. Thus, through a proper design of the PC it is possible to increase the photon absorption in a certain range of wavelengths while keeping the transparency of the complete device. Although this strategy has been experimentally proved with all nanoparticle 1DPC-TiO_2 electrodes [2, 22], the coupling of photonic back reflectors onto nanocolumn based electrodes is still an open challenge, particularly if light scattering effects have to be avoided. Previous attempts in this same direction have focused on the integration of inverse opals onto ZnO nanorod electrodes, for which the device manufacturing process requires a multi-step deposition process [26, 27]. In another approach, a complete structure formed by TiO_2 nanotubes and a 1DPC, which yielded a significant enhancement of the LHE, was prepared by electrochemical anodization [28, 29]. However, this process could

#245708 Received 9 Jul 2015; revised 9 Sep 2015; accepted 5 Oct 2015; published 3 Nov 2015

not be straightforwardly up-scaled because the thin oxidized layer had to be detached from the Ti substrate and then transferred onto a FTO substrate.

Herein we present a novel architecture consisting of a TiO_2-SiO_2 1DPC coupled to a nanocolumnar TiO_2 electrode fabricated in a single-step PV-OAD process. This structure combines materials for which simultaneous optimization of electron transport and photon absorption can be achieved. It also allows controlling the desired extent of porosity, a requisite to optimize electrolyte flow through the photoanode, by taking advantage of the shadowing effects inherent to PV-OAD [30]. Another potential advantage of these photoanodes is the possibility to avoid light dispersion effects by properly adjusting their thickness and microstructure [8]. Our results demonstrate that, in comparison with equivalent cells prepared without any additional photonic structure, rises of up to 39% in photocurrent and 30% in photovoltaic efficiency are obtained with DSCs incorporating 1DPCs, where both the photonic crystal and the photoanode are prepared by PV-OAD. From the perspective of industrial implantation, PVD is advantageous because it can be carried out directly onto the desired substrate –e.g., conductive glass or conductive coated polymer–, provides a precise control over both the thickness and the refractive index of the deposited films and enables the fabrication of 1DPCs with high optical quality over large areas [31–33].

2. Experimental section

2.1 Materials

All commercially available chemicals were used without further purification: ethanol (99.8%, Aldrich), TiO (99.99% from International Advanced Materials) and SiO_2 (Sico Technology GmBH) evaporation targets. Indium-tin oxide (ITO) substrates were purchased from pgo-CEC050S ($\leq 50\ \Omega \cdot sq^{-1}$). The dye (Bu4N)2Ru(debpyH)2(NCS) (Ruthenium 535-bisTBA, also known as N719) and the platinum paste (Platisol-T) were supplied by Solaronix. The electrolyte consisted of a mixture of 100 mM I_2 (Aldrich, 99.999%), 100 mM LiI (Aldrich, 99.9%), 600 mM [(C4H9)4N]I (Aldrich, 98%), and 500 mM 4-tert-butylpyridine (Aldrich, 99%), using 3-methoxy propionitrile (Fluka, ≥99%) as solvent. Surlyn-30 (Dyesol) was used as the hot melt sealing foil. All aqueous solutions were prepared using double distilled and ion-exchanged water.

2.2 Preparation of electrodes

The nanocolumnar TiO_2 electrodes were prepared at room temperature by PV-OAD in an electron bombardment evaporator reactor. TiO was used as target material and stoichiometric layers of TiO_2 were obtained by performing the evaporation in 10-4 torr of O_2 during the deposition. The individual layer thickness was controlled by monitoring the evaporation rate with a previously calibrated quartz crystal monitor. All thin films were prepared with an evaporation rate comprised between 1.0 and 1.5 $Å \cdot s^{-1}$. Flat substrates (ITO glass and Si(100) wafer) were placed at a zenithal evaporation angle (α) of 70° with respect to the evaporation source (see Scheme 1). It has been previously reported that DSC electrodes fabricated at this angle presented the highest performance because the surface area available for adsorption of dye molecules is maximum [8, 10].

The TiO_2 electrode with a zigzag morphology was prepared by turning the substrate 180° around the azimuthal axis (ϕ) each 500 nm until completing the desired thickness. Thereafter, a TiO_2-SiO_2 multilayer was deposited under similar conditions, whereby the SiO_2 layers were prepared using quartz as a target. The substrate was also azimuthally rotated by 180° from one layer to the next. The thicknesses of both the TiO_2 and SiO_2 layers of the photonic crystal, controlled during deposition with a quartz crystal monitor, were carefully adjusted to get a transmission gap that after infiltration with the electrolyte matches the maximum and the higher wavelenghts of the dye absorption band. A set of samples with an increasing number of layers in the 1DPC (8, 10 and 12) was prepared using the described procedure. The as-prepared films were annealed at 400 °C for 4 hours in oxygen flow to induce the crystalline phase transformation of the TiO_2 into anatase.

#245708 Received 9 Jul 2015; revised 9 Sep 2015; accepted 5 Oct 2015; published 3 Nov 2015

2.3 DSC assembly

The prepared samples were immersed overnight in a 0.5 mM dye solution using ethanol as solvent. After immersion they were rinsed with ethanol and dried at 60 °C for 5 minutes. Counter-electrodes were obtained by depositing colloidal platinum paste onto a conductive ITO glass substrate by drop casting and heating at 420 °C for 15 minutes. Both electrodes were sealed using a thermo-polymer. The cells were finally filled with the liquid electrolyte through a hole made previously at the back of the platinized counter-electrode. Then, the hole was sealed with the thermoplastic polymer and a glass cover slide.

2.4 Characterization

The microstructure of the films was characterized by means of a scanning electron microscope (SEM), HITACHI S5200, equipped with a field emission gun. Both planar and cross-section views were obtained for columnar films deposited onto a Si(100) substrate. Cross-section views were obtained by cleaving the samples.

The quasi-normal incidence reflectance spectra were measured with a Bruker IFS-66 FTIR spectrophotometer attached to a microscope with a 4X objective with 0.1 of numerical aperture (light cone angle ± 5.7°).

I–V characterization was carried out with a solar simulator (Sun 2000, Abet Technologies) including a 150W xenon lamp and the appropriate filter for the correct simulation of the 1.5 AM G solar spectrum. The incident light power was normalized to 100 $mW \cdot cm^{-2}$ with a calibrated silicon solar cell. I–V curves were obtained by applying an external bias to the cell and measuring the generated photocurrent with a digital source meter (Keithley 2400). Incident photon to collected electron efficiency (IPCE) measurements were collected with a home-built system composed of a 300W Xenon lamp, a monochromator with 1140 $g \cdot mm^{-1}$ grating (Model 272, McPherson) controlled by a digital scan drive system (Model 789A-3, McPherson), and a picoammeter (Keithley 6485). A UV filter with a cut-off wavelength of 400 nm was used to remove the second order harmonics exiting the monochromator. A silicon photodiode with calibration certificate (D8-Si-100 TO-8 Detector, Sphere Optics) was used to correct the cell response.

3. Results and discussion

The particular deposition geometry used in PV-OAD yields films with an open porous microstructure formed by continuous (i.e., extending from the substrate up to the surface) and tilted nanocolumns [34–38]. This is consequence of the shadowing effects governing the growth mechanism of the films, firstly by the initial nuclei deposited on the surface of the substrate and then by the developing nanocolumns [30, 34–37]. The geometrical characteristics of the nanocolumns can be tuned to get different shapes and orientations (i.e., sculptured thin films) by conveniently moving the substrate during the deposition process using a turntable sample holder. In this way, microstructures in the form of helices [37], vertical rods [39], zigzag [8], sinusoidal [40], or capping [41] can be obtained.

Figure 1(a) presents a cross section SEM micrograph of the structure resulting of the stacking of 12 TiO_2-SiO_2 alternating layers onto a 3 μm thick TiO_2 zig-zag film prepared in one step by PV-OAD. The micrograph clearly shows the six 500 nm segments of TiO_2 electrode film followed by a series of stacked TiO_2-SiO_2 layers, which form the 1DPC structure, also depicting a zigzag configuration. This microstructure is preferred because, although the electron transport and the recombination probability at the oxide-electrolyte interfaces are similar to those of linear nanocolumn arrays [12], the probability to have light scattering is drastically decreased with this configuration, particularly if the photoanode thickness is kept around 3 μm (for higher thicknesses light dispersion effects typical for nanoparticulate DSCs start to be apparent) [8]. The open porous microstructure of the 1DPC-TiO_2 anode eases electrolyte diffusion during device operation [42, 43].

The morphology of the TiO_2-SiO_2 PC is shown in Fig. 1. Backscattered electron micrographs [Fig. 1(a) inset and 1(b) left] of this structure clearly show the two components

#245708 Received 9 Jul 2015; revised 9 Sep 2015; accepted 5 Oct 2015; published 3 Nov 2015

of the multilayer, with the brighter regions corresponding to the material of higher electronic density, i.e., TiO_2. The thickness of TiO_2 and SiO_2 layers was 100 nm and 90 nm, respectively. According to previous studies [31–33], these thickness values maximize the overlapping between the reflection band of the PC and the absorption spectrum of the dye extending up to the IR region of the spectrum. This configuration also maximizes the beneficial effect of the photonic structure on the cell performance [2, 44], as it will be explained below.

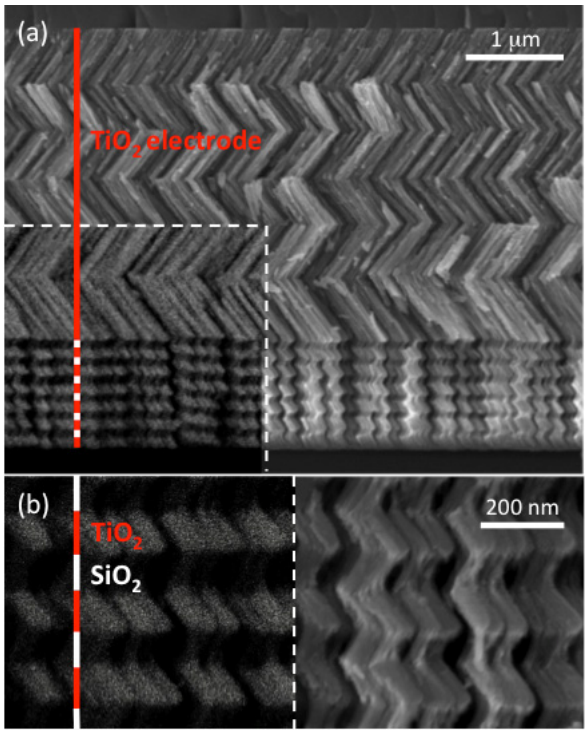

Fig. 1. (a) Cross section secondary electron microscopy image of a 3 μm TiO_2 electrode with a 1DPC structure made of 12 alternated TiO_2-SiO_2 layers. In the left down corner, a micrograph detecting backscattering electrons is overlaid. (b) Backscattered (left) and secondary (right) electron microscopy images showing a detailed cross-section of the photonic structure.

A characteristic feature of 1DPCs is a colored reflection due to light interference phenomena at the interfaces between the different TiO_2 and SiO_2 stacked layers [25, 31]. The characteristic Bragg reflection peaks of the PV-OAD PCs formed by 8, 10 and 12 stacked layers coupled to a 3 μm nanocolumnar TiO_2 electrode were monitored by specular reflectance spectroscopy. Figure 2(a) shows the spectra recorded under quasi-normal incidence illumination from the air-multilayer interface side. It is known that the reflection intensity of 1DPCs increases with the number of layers [31, 45]. For the reported 1DPC structures, it significantly increases from 8 to 10 layers, but only a minor improvement is observed for the 12 layer mirror. Since maximum overlapping with the dye absorption band renders the highest enhancement in the performance of cells incorporating thin electrodes and low dye loadings [44], the thickness of the constituent layers of the bare 1DPC were designed so that the final spectral position and width of the reflection band matches the targeted range when infiltrated by the electrolyte. Please notice that electrolyte filling of the pore network is expected to cause a red-shift of all spectral features. To realize this design, we considered previously attained refractive index (n) values of the individual layers of the stacking, i.e., n equal 1.70 for nanocolumar TiO_2 and 1.28 for nanocolumnar SiO_2 [31].

The photovoltaic performance of DSCs including these structures was compared with that of a reference cell without 1DPC. The characteristic current-voltage (I-V) curves are shown in

#245708 Received 9 Jul 2015; revised 9 Sep 2015; accepted 5 Oct 2015; published 3 Nov 2015

Fig. 2(b) and the photovoltaic parameters extracted from their analysis presented in Table 1. The obtained current densities (J_{sc}) significantly increase when the photonic crystal structure was incorporated onto the TiO_2 anode. The highest value of this parameter was obtained for the 10 and 12 layer structures (9.24 mA/cm^2 and 9.18 mA/cm^2, respectively), with a photocurrent enhancement of 39% with respect to the reference. This result is consistent with the ΔJ_{sc} values predicted theoretically by Lozano et al. in reference [44], where the dependence of the expected enhancement of J_{sc} with the thickness of the titania electrode and the period of the photonic structure was analyzed. The open circuit voltage (V_{oc}) remained invariant for all the cells with the exception of the 12 layer PC cell that presented a slight decrease, probably due to an increased resistance to electrolyte flow and subsequent increase of recombination rate due to the higher tortuosity of this PC. Thus, the interplay between the improvement of light reflection and the tortuosity hindering effects on diffusion makes that, although the fill factor (FF) of the PC cells decreased, the J_{sc} enhancement resulted in an overall improvement of efficiency (η). The best performance was found for the 10 layer PC cell (η = 3.9%), which reached a 30% enhancement with respect to the reference. This value is significantly higher than that found for DSCs incorporated PV-OAD electrodes of similar or higher thickness [8–12]. Moreover, we want to point out that the values obtained for the DSC reference and for the DSCs including 1DPCs [Table 1] are in the same range than those found in a similar study using nanoparticle electrodes [2], thus revealing the capability of TiO_2 nanocolumnar films as electrodes in photovoltaic applications.

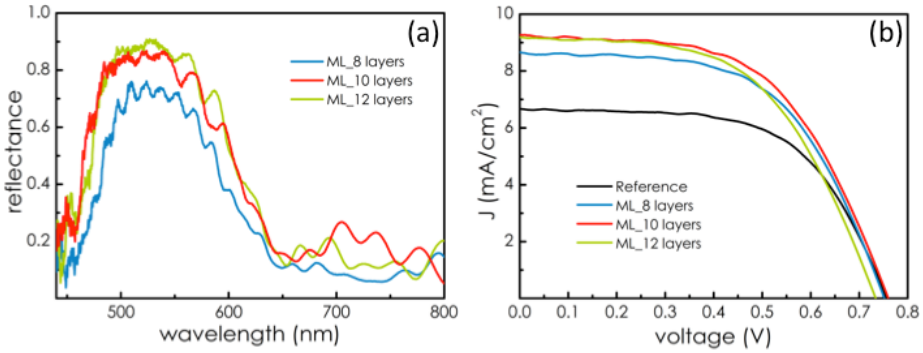

Fig. 2. (a) Specular reflectance spectra of the as-prepared electrodes combining 3 μm of TiO_2 and 1DPC structures with different number of stacked layers. (b) The corresponding I-V curves under standard illumination conditions (100 mW cm^{-2}, AM 1.5 G) of DSCs prepared with the previous structures. The IV curve measured for a DSC made of the same TiO_2 electrode thickness but without photonic structure is also presented as a reference.

Table 1. Photovoltaic parameters extracted from the analysis of I-V curves presented in Fig. 2(b).

Sample	J_{sc} (mA/cm^2)	Voc (V)	FF (%)	η(%)
Reference	6.66	0.756	60.4	3.0
ML_8 layers	8.63	0.752	57.3	3.7
ML_10 Layers	9.24	0.759	56.0	3.9
ML_12 Layers	9.18	0.733	54.9	3.7

To understand the effect of the PC on the optical and photovoltaic properties of the final device, a thorough study was carried out with the 10 layer PC cell. With this purpose, specular reflectance spectra of the DSC were recorded for frontal and rear illumination conditions (see Fig. 3). According to the scheme in Fig. 3(b), under rear illumination the light impinges first on the PC structure and a well-defined Bragg peak can be detected. As mentioned above, the position of this reflection band is red-shifted (see Fig. 3(a) when compared to the spectrum in Fig. 2(a) taken for the same optical structure before its implementation in the cell) due to the change of the effective refractive index of the individual layers constituting the 1DPC upon infiltration with the electrolyte. When the sample is illuminated from the front side (i.e.,

#245708 Received 9 Jul 2015; revised 9 Sep 2015; accepted 5 Oct 2015; published 3 Nov 2015

normal working conditions), the intensity of the reflectance spectrum in the wavelength range matching the dye absorption band (included in Fig. 3(a) for comparison) is strongly suppressed. Related to these effects, a clear niche of application of DSCs contemplates their implementation onto glass in the form of colored layers. The visual appearance of a PV-OAD device and its transparency are illustrated by the transmittance (left) and reflectance (right) pictures presented in Fig. 3(c) for the case in which the 10 layer 1DPC has been included. For comparison, a photograph of a reference cell with the same thickness of TiO_2 layer without the photonic structure is also shown. These images clearly reveal the characteristic color of the Bragg reflector and support the suitability of the 1DPC-DSCs for aesthetic and/or architectural applications.

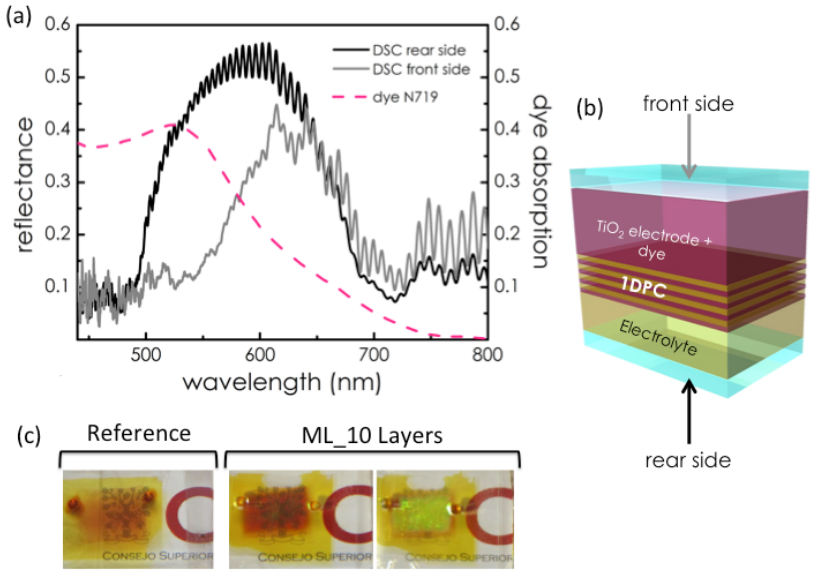

Fig. 3. (a) Specular reflectance spectra of a DSC including a 10 layer PC and a 3 µm TiO_2 nanocolumnar electrode measured from the front and rear sides as it is illustrated in the scheme (b). The dye absorption spectrum is included for comparison. (c) Pictures of a reference and a 10 layers PC DSCs, reporting both the transmittance (left) and the reflectance (right) views are reported.

The clear definition between interfaces for the so prepared photoactive layers gives rise to thin film interference effects that can be detected in a detailed analysis of the spectral photocurrent enhancement factor, defined as the ratio between the IPCE of the 1DPC based cell and that of the reference cell. Results for different electrode thicknesses are presented in Fig. 4 together with the corresponding specular reflectance spectra recorded for the DSCs. The maxima of these two spectra overlap revealing the photonic origin of the improvement observed in the photocurrent for the 1DPC based cells. Also, for the case of the 2 µm thick TiO_2 active layer, a clear correlation between the spectral position of reflectance secondary minima, observed within the photonic band gap frequency range, and the photocurrent enhancement peaks can be observed, as shown in Fig. 4(b). As previously reported, this effect comes from the increased optical field intensity that occurs within the absorbing electrode due to the coupling of the photonic structure [22, 23]. As the number of resonant modes increases with the electrode thickness, their presence is more easily detected in thin electrode architectures.

#245708 Received 9 Jul 2015; revised 9 Sep 2015; accepted 5 Oct 2015; published 3 Nov 2015

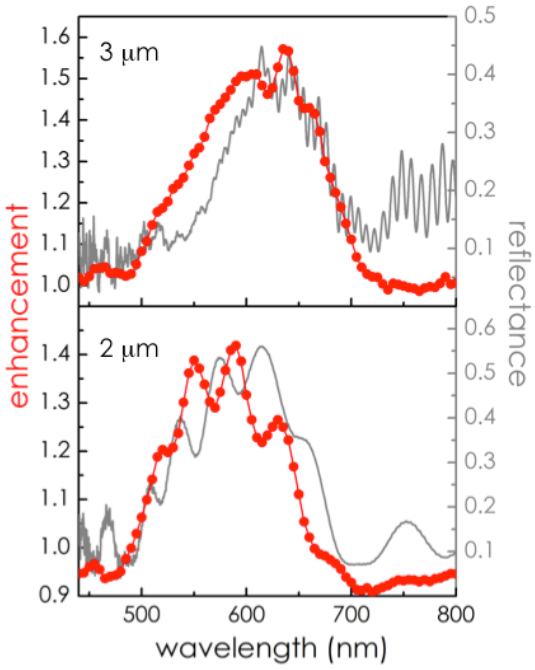

Fig. 4. Specular reflectance spectra of the 10 layer 1DPC DSCs (gray) and the photocurrent enhancement factors (red), defined as the ratio between the IPCE of the 1DPC based cells and that of the reference cell, for the electrode thicknesses indicated.

4. Conclusion

In this work we have reported a one-step fabrication method of zigzag nanostructures formed by a TiO_2-SiO_2 1DPC and a thin film electrode made of aligned TiO_2 nanocomlumnar films grown by PV-OAD. The so-built electrodes present the requested features to allow for optimized charge transport and light harvesting collection, characteristics that to the best of our knowledge have not been achieved in a single structure before. Besides, control over the optical properties of the different stacked layers attained with this technique rendered high quality photonic structures with a characteristic aspect suitable for aesthetic applications in architectural glasses and surfaces. Photovoltaic characterization showed a remarkable improvement of efficiency of the photonic crystal based cells when compared to a nanocolumnar electrode used as reference. IPCE measurements revealed the fingerprint of photon resonant modes in the spectral dependence of the photocurrent, highlighting the photonic origin of the improvement observed. We foresee that the development of a single step physical vapour deposition method to create photoanodes with architectures that synergistically combine the optimum features for both efficient electron transport and light harvesting may have a significant impact in the industrial realization of dye sensitized solar devices.

Acknowledgments

The research leading to the results herein presented has been funded by the European Research Council under the European Union's Seventh Framework Programme (FP7/2007-2013) ERC grant agreement n° 307081 (POLIGHT), the Spanish Ministry of Economy and Competitiveness under grants CONSOLIDER CSD2008-00023 and CSD2007-00007, MAT2011-23593, MAT2013-40852-R and MAT2013-42900-P, and the Junta de Andalucía under Projects TEP8067, FQM-6900, FQM 2265 and FQM 579.

#245708 Received 9 Jul 2015; revised 9 Sep 2015; accepted 5 Oct 2015; published 3 Nov 2015